Turbulent Mixing in Breaking Tidal Bores: Comparison between Field and Laboratory Data

Yit-Haw Toi
The University of Queensland, School of Civil Engineering, Brisbane QLD 4072, Australia.

Hubert Chanson
Professor, The University of Queensland, School of Civil Engineering, Brisbane QLD 4072, Australia.
E-mail: h.chanson@uq.edu.au

ABSTRACT: When a river mouth has a funneled shape with a tidal range exceeding 4 to 6 m, the river may experience a tidal bore, that is a series of waves propagating upstream as the tidal flow turns to rising. Recent studies demonstrated the significant impact of tidal bores on the environmental system and the ecology of the estuarine zone. Herein the unsteady turbulent mixing induced by a breaking tidal bore was documented based upon new physical experiments. Detailed free-surface and velocity measurements were performed with a high-temporal temporal resolution. The physical results were compared systematically with a recent field data set (Mouazé et al. 2010). The propagation of breaking tidal bores was associated with a sharp free-surface discontinuity at the bore front, followed by some transient recirculation next to the bed. A key finding was the close agreement in terms of dimensionless free-surface and velocity data between laboratory and field observations.

KEY WORDS: Breaking tidal bores, Field data, Froude similitude, Physical modelling, Unsteady turbulent mixing.

1 INTRODUCTION

A tidal bore is a surge of waters propagating upstream as the tidal flow turns to rising and the flood tide rushes into a funnel shaped river mouth with shallow waters (Tricker 1965). The bore forms during the spring tides when the tidal range exceeds 4 to 6 m and the estuary bathymetry amplifies the tidal range with a low freshwater level. It is estimated worldwide that over 400 estuaries are affected by a tidal bore, on all continents but Antarctica (Chanson 2011). Figure 1 shows six photographs of a tidal bore and following flood tide motion, all within 20 minutes. The sequence highlights the rapid advance of the flow, the intense turbulence of the breaking roller and the rapid rise in water elevation during the early flood tide (see survey staff in last three photographs). Recent studies demonstrated the significant impact of tidal bores on the environmental system and the ecology of the river mouth. Surprisingly many hydrodynamic features remain unexplained, and field data sets are limited despite a few successful ones.

The interactions between tidal bores and human society are complex A tidal bore impacts on a range of socio-economic resources, encompassing the sedimentation of the upper estuary, the impact on the reproduction and development of native fish species, and the sustainability of unique eco-systems (Rowbotham 1983, Rulifson and Tull 1999, Chanson 2011). A tidal bore can be a major tourism attraction like in North America, Far East Asia and Europe. A number of bores are surfed with tidal bore surfing competitions and festivals in South America, Europe and South-East Asia. But a tidal bore is a massive hydrodynamic shock which might become dangerous and hinder the local traffic and development. A bore is an integral part of the environmental and socio-cultural heritage It is a fascinating geophysical phenomenon in terms of geo-morphological and biological processes, as well as for the estuarine populations.

A related process is the tsunami-induced bore. When a tsunami wave propagates in a river, its leading edge is led by a positive surge. The tsunami-induced bore may propagate far upstream. Some tsunami-induced river bores were observed in Hawaii in 1946, in Japan in 1983, 2001, 2003 and 2011, and even in the River Yealm in United Kingdom on 27 June 2011 (Tanaka et al. 2008, Wijetunge et al. 2008). During the 11 March 2011 tsunami catastrophe in Japan, tsunami-induced bores were observed in several rivers in north-eastern Honshu and as far as North-America (Adityawan et al. 2012).

In this study, the unsteady turbulence and turbulent mixing induced by a breaking tidal bore were documented based upon new physical experiments. Detailed free-surface and velocity measurements were performed with a high-temporal resolution (200 Hz) using non-intrusive free-surface measurement probes and side-looking acoustic Doppler velocimetry. The physical results were then compared systematically with a recent field data set conducted in the breaking bore of the Sélune River (France) by Mouazé et al. (2010).

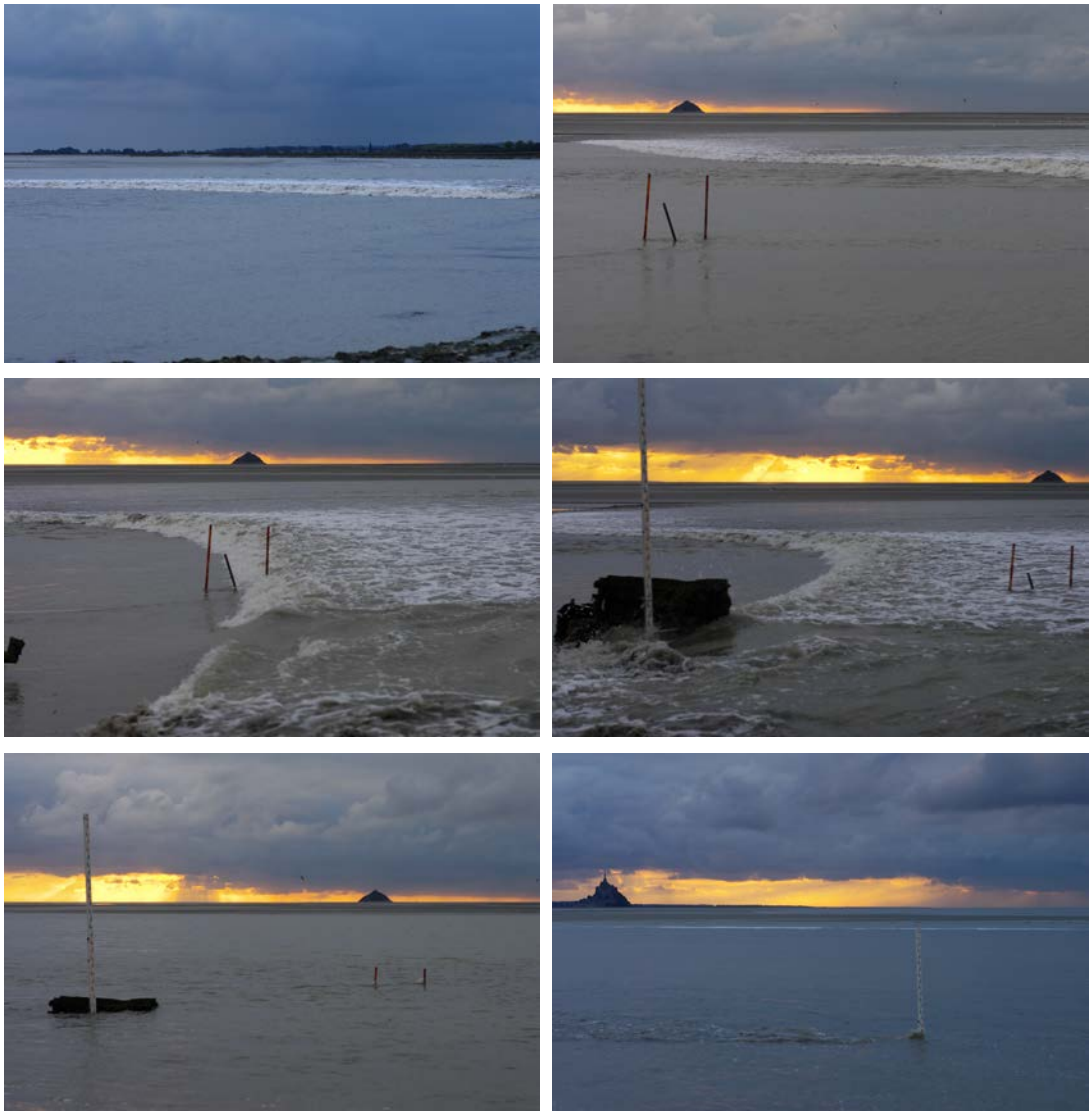

Figure 1 Breaking tidal bore of the Sélune River (France) on 24 September 2010 - From Left to right, top to bottom: 19:21:51, 19:30:09, 19:30:16, 19:30:17, 19:32:02, 19:40:23 (French local time)

2 STUDY METHODS

2.1 Dimensional analysis

Any laboratory study of tidal bores requires the selection of a suitable similitude. The relevant parameters for a dimensional analysis include the fluid properties and physical constants, the channel geometry, and the initial and boundary conditions (Docherty and Chanson 2012). For a tidal bore propagating in a horizontal prismatic rectangular channel, a simplified dimensional analysis gives a series of relationships between the dimensionless unsteady flow properties as functions of a number of relevant dimensionless numbers:

$$\frac{P}{\rho\,g\,d_o}, \frac{V_x}{V_o}, \frac{V_y}{V_o}, \frac{V_z}{V_o} = F\left(\frac{x}{d_o}, \frac{y}{d_o}, \frac{z}{d_o}, t\sqrt{\frac{g}{d_o}}, \frac{V_o+U}{\sqrt{g d_o}}, \rho\times\frac{(V_o+U)\,d_o}{\mu}, \frac{g\,\mu^4}{\rho\,\sigma^3}, \frac{B}{d_o}, ...\right) \quad (1)$$

where P is the instantaneous pressure, V_x, V_y, V_z are respectively the longitudinal, transverse and vertical velocity components at a location (x, y, z) at a time t, x is the coordinate in the flow direction, y is the horizontal transverse coordinate measured from the channel centreline, z is the vertical coordinate measured from channel bed, U is the surge celerity, d_o and V_o are the initial flow depth and velocity respectively, B is the channel width, g is the gravity acceleration, ρ and μ are the water density and dynamic viscosity respectively, and σ is the surface tension between air and water. In addition, the biochemical properties of the water solution may be considered especially in natural estuarine systems.

In Equation (1), right handside, the 5th, 6th and 7th terms are respectively the Froude, Reynolds and numbers. Basic momentum considerations demonstrate the significance of the Froude number (Bélanger 1841, Lighthill 1978), and the selection of a Froude similitude follows implicitly from basic theoretical considerations (Liggett 1994, Chanson 2012). When the same fluids (air and water) are used in the field and laboratory, the Froude and Morton similarities are simultaneously used. In turn the Reynolds number may be grossly underestimated in laboratory conditions, thus leading to viscous scale effects in small size models typical of hydraulic engineering applications.

2.2 Laboratory experiments and instrumentation

New experiments were performed in a 12 m long 0.5 m wide tilting flume previously used by Koch and Chanson (2009). The channel was made of smooth PVC bed and glass walls (Fig. 2). A tainter gate was located at x = 11.15 m where x is the longitudinal distance from the test section upstream end. The tainter gate was a fast closing gate, with a closing time of less than 0.15 s. The gate closure generated a bore propagating upstream against an initially steady flow.

The water flow rate was supplied by a constant head tank and measured with an orifice meter calibrated in-situ. In steady flows, the flow depth was measured with a series of pointer gauges. The unsteady water depths were recorded using acoustic displacement meters Microsonic™ Mic+25/IU/TC, with a dynamic response time of less than 50 ms. The instantaneous velocity components were measured with an acoustic Doppler velocimeter (ADV) Nortek™ Vectrino+, equipped with a side-looking head. The translation of the ADV probe in the vertical direction was controlled by a fine adjustment travelling mechanism connected to a Mitutoyo™ digimatic scale unit. The ADV sampling volume was located at x = 4.5 m on the channel centreline. (The ADV stem is seen in Figure 2.) Both the acoustic displacement meters and ADV were sampled simultaneously and synchronously at 200 Hz.

The experimental setup and flow conditions were selected to generate both breaking and undular breaking tidal bores with the same initial flow rate, although the present study focused mostly on breaking bores. The only dependant parameter was the tainter gate opening (after closure) and the experimental flow conditions are summarised in Table 1.

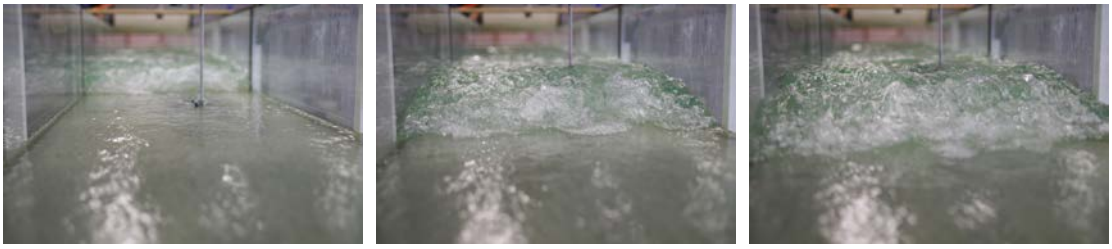

Figure 2 Breaking bore propagation in laboratory, looking downstream (Fr_1 = 2.1)

Table 1 Experimental investigations of and velocity measurements in breaking tidal bores

Reference	Q (m^3/s)	S_o	Bed roughness	d_o (m)	V_o (m/s)	Fr	$\rho\frac{(V_o+U)\,d_o}{\mu}$	Instrument
Field studies								
Simpson et al.	N/A	N/A	Mobile bed & bed	0.72	0.15	1.8	3.0×10^6	ADCP.
Mouazé et al. (2010)	N/A	N/A	Mobile bed ('tangue')	0.375 0.325	0.86 0.59	2.35 2.48	1.1×10^6 8.2×10^5	ADV.
Laboratory studies								
Chanson (2010)	0.058	0	Smooth PVC	0.139	0.832	1.50	2.4×10^5	ADV.
			Rough screen	0.141	0.824	1.46	2.4×10^5	
Docherty and Chanson (2012)	0.050	0.0	Smooth PVC	0.118	0.848	1.59	2.0×10^5	ADV.
		0.002	Fixed gravel	0.126	0.794	1.49	2.1×10^5	
Present study	0.025	0.0035	Smooth PVC	0.0517	0.966	2.10	7.7×10^4	ADV.
				0.0514	0.973	2.02	7.3×10^4	
				0.0519	0.963	1.91	7.0×10^4	
				0.0508	0.973	1.74	6.2×10^4	

Notes: Q: initial steady flow rate; S_o: bed slope; d_o, V_o: initial flow depth and velocity recorded at sampling location; U: tidal bore celerity positive upstream on the channel centreline; Fr: tidal bore Froude number.

3 RESULTS AND DISCUSSION

3.1 Flow patterns

The tidal bore propagation and its shape were closely linked with the Froude number $Fr = (V_o+U)/(g\,A_o/B_o)^{1/2}$ where U is the bore celerity positive upstream, and A_o and B_o are respectively the initial flow cross-section area and free-surface width. For Fr < 1.7, the bore front was smooth and followed by a train of pseudo-periodic undulations. For Fr > 1.7, the bore had a marked roller (i.e. breaking front) which extended across the whole channel width, as illustrated in Figure 2. The roller size and its strength appeared to increase with increasing Froude number. The roller toe was a flow singularity: both air entrapment and intense turbulent mixing were generated at the toe, with increasing mixing and air entrainment in the roller with increasing Froude number. The visual observations were consistent with the results of Favre (1935), Benet and Cunge (1971), Hornung et al. (1995), Koch and Chanson (2009) and Chanson (2010).

In the system of references in translation with the bore, the continuity and momentum principles give a relationship between the flow properties in front of and behind the bore (Liggett 1994, Chanson 2012):

$$\frac{A_{conj}}{A_o} = \frac{1}{2}\,\frac{\sqrt{\left(2-\frac{B'}{B}\right)^2 + 8\,\frac{B'/B}{B_1/B}\,Fr^2} - \left(2-\frac{B'}{B}\right)}{\frac{B'}{B}} \quad (2)$$

where A is the channel cross-sectional area measured perpendicular to the main flow direction, the subscript o refers to the initial flow conditions, the subscript conj refers to the conjugate flow conditions immediately after the bore, and B and B' are characteristic widths. Equation (2) is valid for any tidal bore in an irregular prismatic channel (Chanson 2012); in a rectangular prismatic channel, it simplifies into the Bélanger equation. The present data are presented in Figure 3 and they are compared with a range of physical data. The results showed a good agreement between all physical data, including field data. In Figure 3, the two data sets on the top right are those of the Sélune River bore (Mouazé et al. 2010) in a very shallow, wide channel seen in Figure 1, for which the effects of the channel cross-sectional shape were substantial.

Some typical roller length data are reported in Figure 4, in which the bore roller data are compared with stationary hydraulic jump data. The results indicated an increasing roller length with increasing Froude number, but for the Sélune River bore data. No physical justification is available to explain the discrepancy with laboratory data.

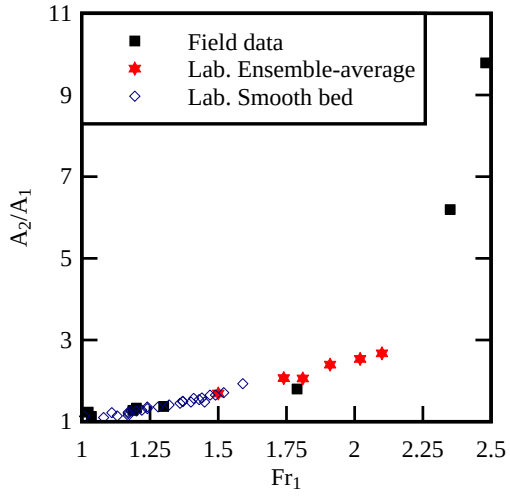

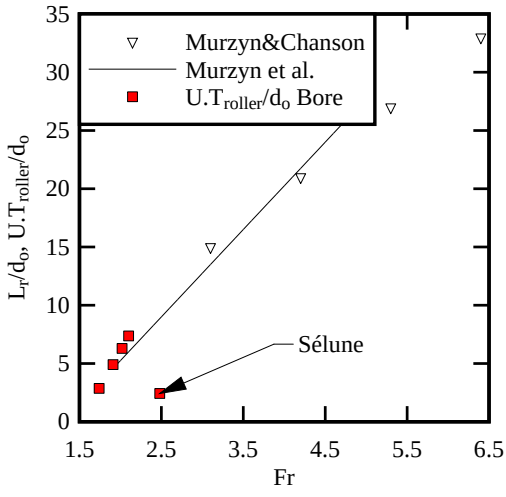

Figure 3 (Left) Relationship between the ratio of conjugate cross-section areas and Froude number - Comparison between field data (Chanson et al. 2011, Mouazé et al. 2010, Reungoat et al. 2012, Simpson et al. 2004, Wolanski et al. 2004), ensemble-averaged laboratory data (Docherty and Chanson 2012, Present study) and single-run laboratory data (Chanson 2010, Koch and Chanson 2009)

Figure 4 (Right) Dimensionless roller length in breaking tidal bores - Comparison between prototype data (Mouazé et al. 2010), laboratory data (Present study) and stationary hydraulic jump data (Murzyn et al. 2007, Murzyn and Chanson 2009)

3.2 Velocity measurements

The velocity data indicated the marked impact of the breaking bore propagation on the velocity field (Fig. 5). Figure 5a shows the time-variations of the water depth and longitudinal velocity component at three vertical elevations during the breaking bore propagation in laboratory, where the longitudinal velocity component V_x is positive downstream. The tidal bore passage was characterised by a rapid rise in the free surface elevation, corresponding to the bore roller, which was associated with a sharp flow deceleration at all vertical elevations (Fig. 6). Figure 6 shows the vertical distributions of the maximum longitudinal flow deceleration, calculated based upon the low-pass filtered longitudinal velocity component. The flow deceleration was 0.14×g on average. The laboratory data compared favourably with the field data in the Sélune River bore, in which a maximum deceleration of about 0.16×g was recorded (Fig. 6).

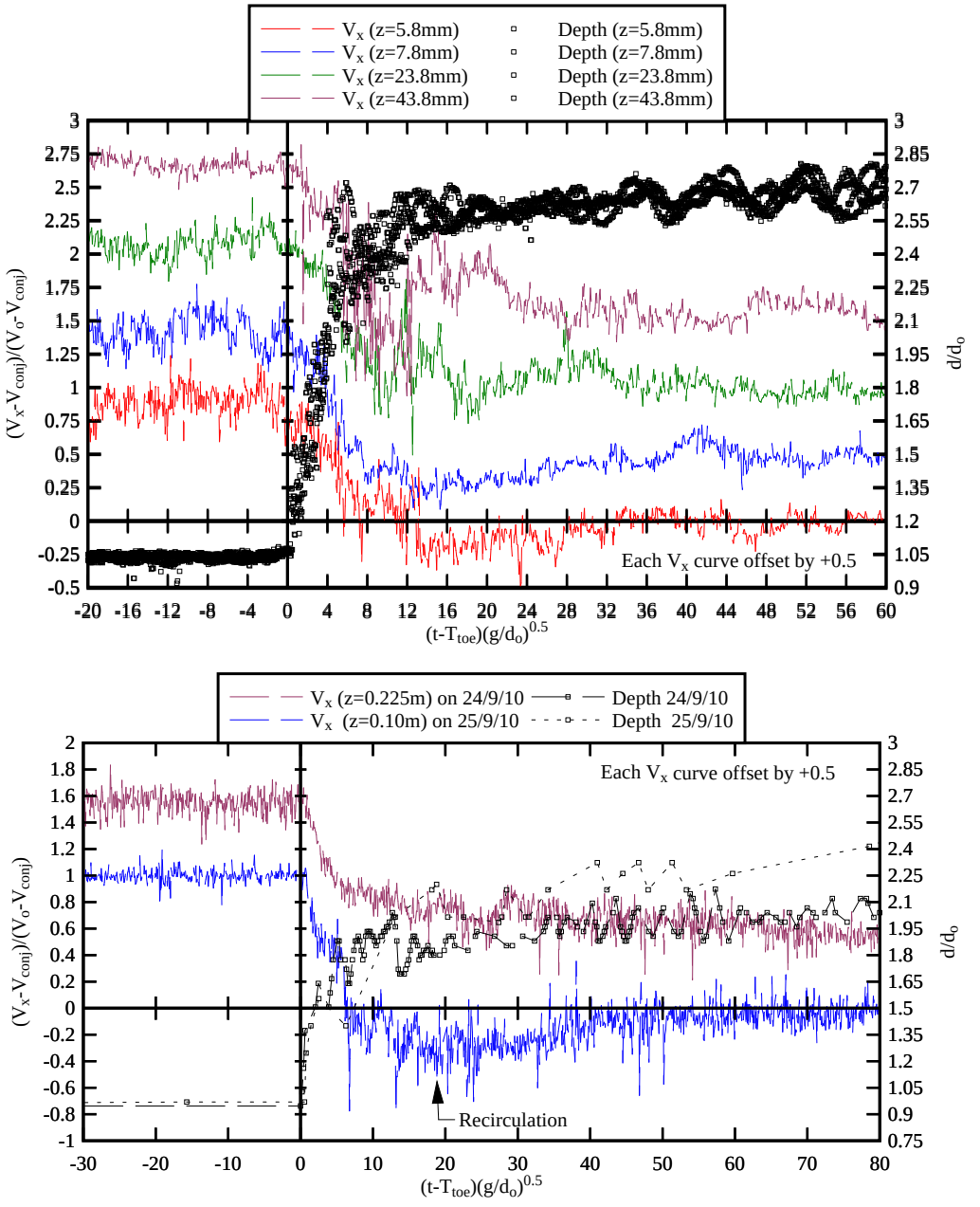

Figure 5 Time-variations of water depth and longitudinal velocity components in breaking bores - Comparison between (a, top) laboratory data at z/d_o = 0.11, 0.15, 0.46 & 0.85 (d_o = 0.0514 m, Fr = 2.0, Present study)) and (b, bottom) field data at z/d_o = 0.31 & 0.65 (d_o = 0.325 m, Fr = 2.5, Mouazé et al. 2010)

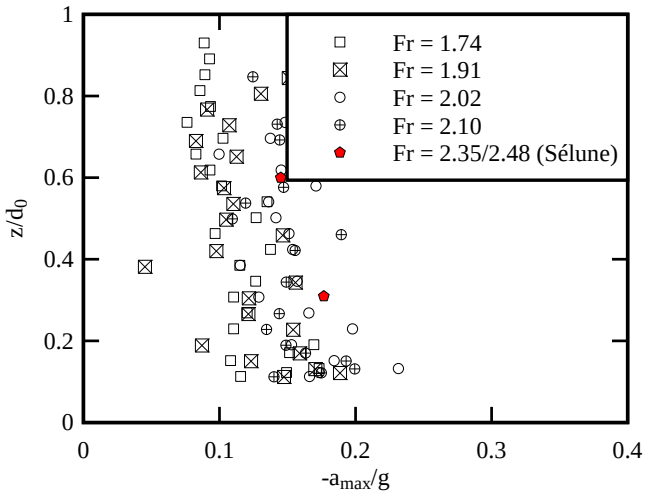

Figure 6 Vertical distribution of longitudinal flow deceleration in breaking tidal bores - Comparison between prototype data (Sélune River, Mouazé et al. 2010) and laboratory data (Present study)

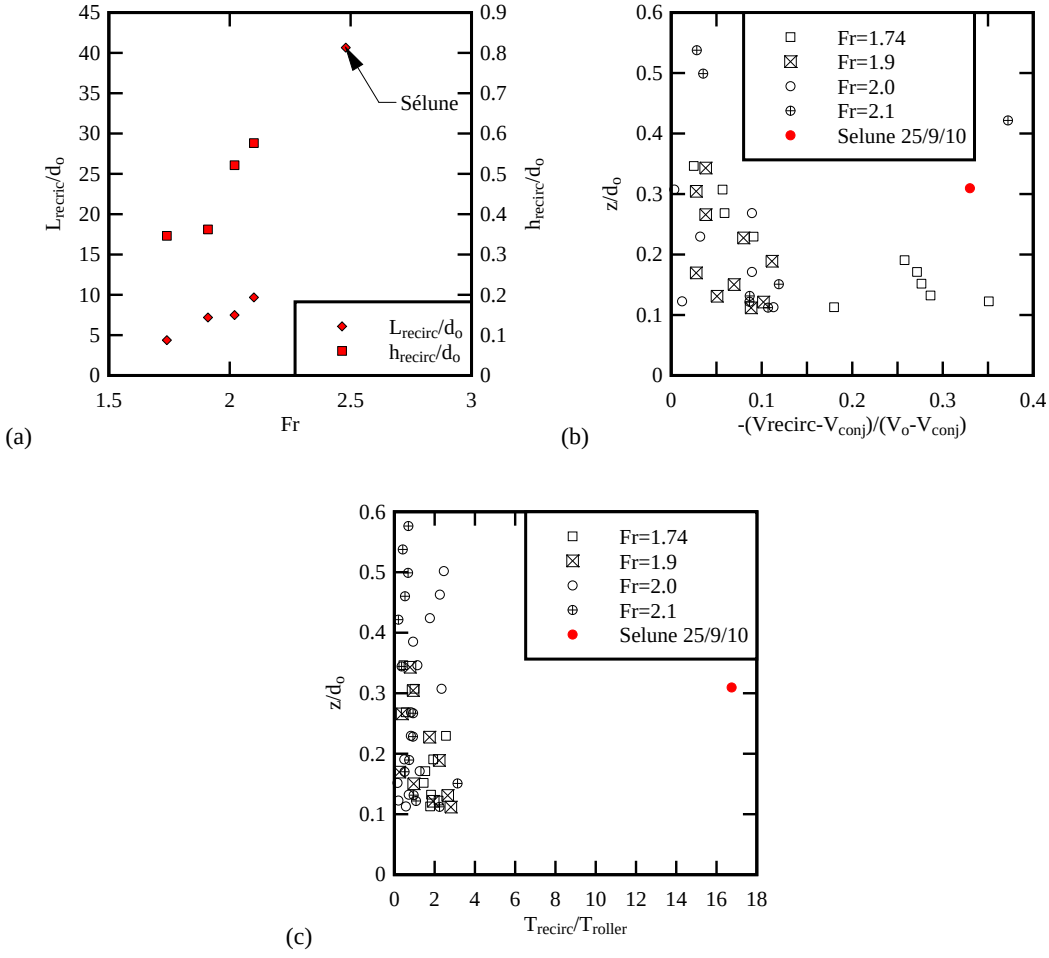

Figure 7 Characteristics of transient recirculation beneath breaking tidal bores: (a) recirculation bubble length and height, (b) maximum recirculation velocity amplitude, (c) duration of transient recirculation

The laboratory velocity measurements (Fig. 5a) presented a data trend comparable to the field observations of Mouazé et al. (2010) in the Sélune River bore (Fig. 5b), for a similar relative elevation z/d_o. This is seen in Figure 5 presenting the time-variations of the instantaneous longitudinal velocity component, where V_{conj} is the conjugate flow velocity. The findings were consistent with the data of Simpson et al. (2004) in the Dee River bore, and Hornung et al. (1995), Koch and Chanson (2009) and Chanson (2010) in laboratory channels. The upstream propagation of breaking tidal bores was characterised by large fluctuations of all velocity components beneath and behind the bore roller. A basic flow feature was the transient recirculation close to the bed behind the roller, which is highlighted in Figure 5a and 5b. Such an unsteady recirculation was observed in breaking bores, but not beneath undular bores.

For the laboratory experiments, the velocity measurements showed that the amplitude of maximum recirculation velocity decreased with increasing distance from the channel bed. The characteristics of the transient recirculation flow region are summarised in Figure 7: i.e., the maximum height h_{recirc} and length L_{recirc} of the recirculation bubble, the maximum recirculation velocity amplitude V_{recirc}, and the duration T_{recirc} of the transient recirculation. Both laboratory and field data are presented in Figure 7. The observations showed that the dimensions of transient recirculation region and the maximum recirculation velocity amplitude increased with increasing Froude number. The maximum recirculation was typically observed shortly after the bore roller in laboratory. The field data in the Sélune River indicated a comparatively longer recirculation zone (Fig. 7), which might be linked with changes in the movable boundaries during the tidal bore propagation.

4 DISCUSSION

The comparison between laboratory and field data highlighted some limitations of the experimental methods, because of differences in the initially-steady flow conditions. In the Sélune River on 24 September 2010, the initially-steady flow Froude number was equal to 0.71 prior to the bore: that is, the river flow was transcritical and some small free-surface standing waves were seen. At the sampling elevation z/d_o = 0.6, the time-averaged longitudinal velocity V_x equalled +0.98 m/s, and the dimensionless velocity standard deviations were equal to: v_x'/V_x = 0.16, v_y'/V_x = 0.04, and v_z'/V_x = 0.14. In the present laboratory study, the data yielded the following initially-steady turbulent flow conditions at z/d_o = 0.6: V_x = +1.08 m/s, v_x'/V_x = 0.068, v_y'/V_x = 0.032, and v_z'/V_x = 0.12 for Fr = 2.1. Despite these differences in inflow conditions and the Sélune River channel's movable boundaries, the present analysis showed some close agreement in terms of dimensionless free-surface and velocity data between laboratory and field observations (Fig. 5). The finding is important because it does support the physical approach undertaken herein as well as in previous studies.

Khezri and Chanson (2012) studied the sediment motion beneath a breaking bore in laboratory, with the sediment inception being linked with the longitudinal pressure gradient $\partial P/\partial x$, while the upstream particle motion was driven by the transient drag force during the transient recirculation. In their experiments, the median maximum particle acceleration was 0.4×g, with 10% of particles reaching longitudinal acceleration in excess of 1×g. These acceleration levels were significantly greater than the flow deceleration measurements reported herein (Fig. 6). The finding may reflect upon the predominant role of the longitudinal pressure gradient to destabilise and accelerate the bed sediment material.

Both field measurements and laboratory studies highlighted some basic features of the impact of breaking tidal bores on the estuarine system. The turbulent velocity measurements indicated the existence of energetic turbulent events during and behind the tidal bore. These are highlighted by large and rapid f1uctuations of instantaneous velocities and Reynolds stresses. The duration of the turbulent events seemed more intense beneath breaking bores. This type of macro-turbulence can maintain its coherence as the eddies are advected behind the bore. Importantly the macro-turbulence may contribute to significant sediment erosion from the bed and banks, and the upstream advection of the eroded material as illustrated in Figure 8.

More generally the bore occurrence is essential to a number of ecological processes and the sustainability of unique eco-systems. The tidal bore propagation induces a massive mixing of estuarine waters stirring the organic matter and creating some rich fishing grounds: for example, the Rokan River in Indonesia.

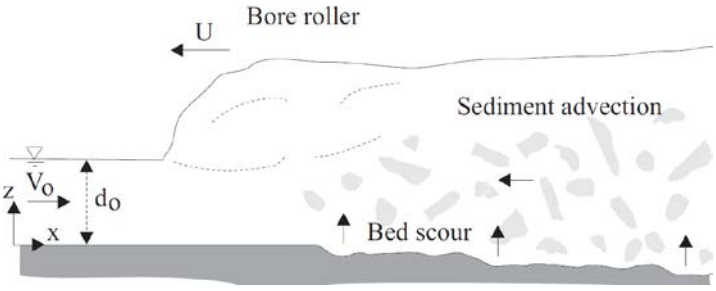

Figure 8 Conceptual sketch of bed scour beneath and upstream sediment advection behind a breaking tidal bore

5 CONCLUSION

A tidal bore is a hydrodynamic shock propagating upstream as the tidal flow turns to rising. The tidal bore propagation induces a massive mixing of the natural system. Its occurrence is critical to the environmental balance of the estuarine zone. The present study focused on the unsteady turbulence induced by a breaking tidal bore. New experiments were conducted under controlled flow conditions in a relatively large flume. Detailed free-surface and velocity measurements were performed using non-intrusive free-surface measurement probes and side-looking acoustic Doppler velocimetry. The laboratory data were compared systematically with some field measurements conducted in the breaking bore of the Sélune River in France (Mouazé et al. 2010). The propagation of a breaking bore was associated with a sharp free-surface discontinuity at the bore front, followed by intense velocity fluctuations and some transient recirculation next to the bed. The flow properties upstream and downstream of the bore front fulfilled some basic momentum consideration. The passage of breaking bores is associated with large fluctuations in water depth and instantaneous velocity components. This is associated with intense turbulent mixing, and sediment scour and advection in a natural estuarine system. A key finding was the close agreement in terms of dimensionless free-surface and velocity data between laboratory and field observations. This was never been tested to that level to date.

ACKNOWLEDGEMENTS

The writers acknowledge the technical assistance of Ahmed Ibrahim and Jason Van Der Gevel (The University of Queensland), and the financial of the University of Queensland, the Université de Bordeaux (I2M), the Australian Academy of Science and the Agence Nationale de la Recherche (Projet 10-BLAN-0911-01).

References

Adityawan MB, Roh M, and Tanaka H (2012) Investigation of tsunami Propagation Characteristics in River and on Land Induced by the Great East Japan Earthquake 2011. Journal of Earthquake and Tsunami, Vol. 6, No. 3, Paper 1250033, 22 pages (DOI: 10.142/S1793431112500339).

Bélanger JB (1841) Notes sur l'Hydraulique. Ecole Royale des Ponts et Chaussées, Paris, France, session 1841-1842, 223 pages (in French).

Benet F, and Cunge JA (1971) Analysis of Experiments on Secondary Undulations caused by Surge Waves in Trapezoidal Channels. Jl of Hyd. Res., IAHR, 9(1):11-33.

Chanson H (2010) Unsteady Turbulence in Tidal Bores: Effects of Bed Roughness. Journal of Waterway, Port, Coastal, and Ocean Engineering, ASCE, 136(5): 247-256 (DOI: 10.1061/(ASCE)WW.1943-5460.0000048).

Chanson H (2011) Tidal Bores, Aegir, Eagre, Mascaret, Pororoca: Theory and Observations. World Scientific, Singapore, 220 pages (ISBN 9789814335416).

Chanson H (2012) Momentum Considerations in Hydraulic Jumps and Bores. Journal of Irrigation and Drainage Engineering, ASCE, 138(4): 382-385 (DOI 10.1061/(ASCE)IR.1943-4774.0000409).

Chanson H, Reungoat D, Simon B, and Lubin P (2011) High-Frequency Turbulence and Suspended Sediment Concentration Measurements in the Garonne River Tidal Bore. Estuarine Coastal and Shelf Science, 95(2-3): 298-306 (DOI 10.1016/j.ecss.2011.09.012).

Docherty NJ, and Chanson H (2012) Physical Modelling of Unsteady Turbulence in Breaking Tidal Bores. Journal of Hydraulic Engineering, ASCE, Vol. 138, No. 5, pp. 412-419 (DOI: 10.1061/(ASCE)HY.1943-7900.0000542).

Favre H (1935) Etude Théorique et Expérimentale des Ondes de Translation dans les Canaux Découverts. Dunod,

Paris, France (in French).
Hornung HG, Willert C, and Turner S (1995) The Flow Field Downsteam of a Hydraulic Jump. Jl of Fluid Mech., 287:299-316.
Khezri N, and Chanson H (2012) Inception of Bed Load Motion beneath a Bore. Geomorphology, 153-154:39-47 (DOI: 10.1016/j.geomorph.2012.02.006).
Liggett JA (1994) Fluid Mechanics. McGraw-Hill, New York, USA.
Lighthill J (1978) Waves in Fluids. Cambridge University Press, Cambridge, UK, 504 pages.
Koch C, and Chanson H (2009) Turbulence Measurements in Positive Surges and Bores. Jl of Hyd. Res., IAHR, 47(1):29-40 (DOI: 10.3826/jhr.2009.2954).
Mouazé D, Chanson H, and Simon B (2010) Field Measurements in the Tidal Bore of the Sélune River in the Bay of Mont Saint Michel (September 2010). Hydraulic Model Report No. CH81/10, School of Civil Engineering, The University of Queensland, Brisbane, Australia, 72 pages.
Murzyn F, and Chanson H (2009) Free-Surface Fluctuations in Hydraulic Jumps: Experimental Observations. Experimental Thermal and Fluid Science, Vol. 33, No. 7, pp. 1055-1064 (DOI: 10.1016/j.expthermflusci.2009.06.003).
Murzyn F, Mouazé D, and Chaplin JR (2007) Air-Water Interface Dynamic and Free Surface Features in Hydraulic Jumps. Jl of Hydraulic Res., IAHR, 45(5):679-685.
Reungoat, D., Chanson, H., and Caplain, B. (2012) Field Measurements in the Tidal Bore of the Garonne River at Arcins (June 2012). Hydraulic Model Report No. CH89/12, School of Civil Engineering, The University of Queensland, Brisbane, Australia, 121 pages.
Rowbotham F (1983) The Severn Bore. David & Charles, Newton Abbot, UK, 3rd edition, 104 pages.
Rulifson RA, and Tull KA (1999) Striped Bass Spawning in a Tidal Bore River: the Shubenacadie Estuary, Atlantic Canada. Trans. American Fisheries Soc., Vol. 128, pp. 613-624.
Simpson JH, Fisher NR, and Wiles P (2004) Reynolds Stress and TKE Production in an Estuary with a Tidal Bore. Estuarine, Coastal and Shelf Science, Vol. 60, No. 4, pp. 619-627.
Tanaka H, Ishono K, Nawarathna B, Nakagawa H, Yano S-I, Yasuda H, Watanabe Y. and Hasegawa K (2008) Field Investigation Of Disasters In Sri Lankan Rivers Caused By Sumatra Earthquake Tsunami." J. Hydraulics, Hydrology and Environment, JSCE, 26(1), 91-112.
Tricker RAR (1965) Bores, Breakers, Waves and Wakes. American Elsevier Publ. Co., New York, USA.
Wijetunge JJ, Wang X, and Liu PLF (2008) Indian Ocean Tsunami on 26 December 2004: Numerical Modeling of Inundation in Three Cities on the South Coast of Sri Lanka. Journal of Earthquake and Tsunami, Vol. 2, No. 2, pp. 133-155.
Wolanski E, Williams D, Spagnol S, and Chanson H (2004) Undular Tidal Bore Dynamics in the Daly Estuary, Northern Australia. Estuarine, Coastal and Shelf Science, Vol. 60, No. 4, pp. 629-636.